BALKAN PHYSICS LETTERS
©Bogazici University Press 07 July 2012
BPL, 20, 201039, pp. 328 - 348

# INVARIANT MASS DISTRIBUTIONS OF $\vec{d}(\vec{e},e')$ FROM BLAST

B. T. TONGUC
Physics Department, Sakarya University,
Adapazari, Sakarya, TURKEY.

S. CITCI
Physics Department, Sakarya University,
Adapazari, Sakarya, TURKEY.
M. BEKTASOGLU
Physics Department, Sakarya University,
Adapazari, Sakarya, TURKEY.
and
R. ALARCON
Physics and Astronomy Department, Arizona State University,
Tempe, AZ, USA.

**Abstract.** The BLAST (Bates Large Acceptance Spectrometer Toroid) Experiment was carried out at MIT BATES Linac Center at Middleton, MA, from 2003 to 2005. In the experiment, polarized electrons, accelerated to 850 MeV through Bates Linac, were sent either to polarized hydrogens or to polarized deuteriums at rest. For this study, ~273 MB in size or equivalently ~8 hours long polarized electron-polarized deuteron data taken in 2004 was used. The BLAST spectrometer, used for charged particle tracking, has left-right symmetry relative to beam direction, and consists of drift chambers for position, charge and momentum of particles, Čerenkov counters for electron-pion separation, time-of-flight (TOF) scintillators for duration of time and neutron walls for quasi-elastic scattering off the neutron detection [1]. Once each kinematic quantity in BLAST is matched to the corresponding parameter in crunched data, analysis is made according to perpendicular and parallel cases. Because the dominant interaction channel is electromagnetic, three ( $\vec{q}$ ) and four momentum ( $Q$ ) vectors are transferred from incident electron to one of the nucleon ( $N$ ) in deuteron target by a virtual photon ( $\gamma$ ). In this study, first, these momentum vectors were checked with the data. Second, depending on 4-momentum transfer, invariant mass ( $W$ ) of photon-nucleon ( $\gamma N$ ) system is calculated and its histogram is drawn for each case. Last, these spectra are investigated for $0.1-0.2\ (\mathrm{GeV/c})^2$, $0.2-0.3\ (\mathrm{GeV/c})^2$, $0.2-0.3\ (\mathrm{GeV/c})^2$, and $0.4<(\mathrm{GeV/c})^2$ sub-ranges of $Q^2$. Theoretical calculations and data are seen to be compatible. As a result, upcoming analyses were decided to persue based on this work.

**Key Words:** Invariant mass, Polarized target, Electron-deuteron scattering, Squared 4-momentum transfer, Electromagnetic interaction.

## 1. Introduction

Some of the nucleon-nucleon or electron-nucleon scattering experiments generally is performed for investigating nucleons structure. Particles are accelerated through linear or circular accelerators up to a certain energy are sent to target for collision. These studies beside an accelerator, requires a station equipped with detector systems surrounding the collision region. Detector systems detect particles passing through them and consist of various detector types. Each detector type can have different detection mechanism depending on the particle to detect and its physical quantities to be obtained. Outputs of the detectors are basically analog signals which has to be digitized in order to save the information or raw data for analysis. Digitisation is done through analog-to-digital converters (ADCs)[2]. Data are made ready for analysis by processing the raw data. The process is called "crunching". Data for analysis consist of files. Each file contains data about 27 MB in size corresponding about 50 minutes long data taking at BLAST, an electron-nucleon scattering experiment over hydrogen or deuterium target performed at South Hall Ring of Bates Linear Accelerator Center of Massacchussets Institute of Technology (MIT) between 2003 and 2005. For this study, ~273 MB in size or equivalently ~8 hours long polarized electron-polarized deuteron data taken in 2004 was used.

## 2. BLAST Spectrometer

Information related to position, time, angle, momentum, charge etc. of particles outcoming was obtained by BLAST Spectrometer. BLAST system does not have a $4\pi$ spherical geometry. However, it has a left–right symmetry according to beam line (Figure 1) [4]. The kinematics of analyses based on electrons scattered on the left is called perpendicular kinematics since the angle between the virtual photon momentum and the target polarization orientation $\theta^* \approx 90^0$ while the kinematics of analyses based on electrons scattered on the right is called paralel kinematics since $\theta^* \approx 0^0$. The system from inside to outside consists of wire chambers for particle tracking, Čerenkov counters for electron-pion seperation, Time-of-Flight Scintillators (TOF) for timing and neutron counters for neutron detection, respectively. Among these, only neutron counters aren't symmetrical and information from these is not required for this study. Beside these detectors, there is a toroidal magnet producing up to 2kG field normal to the particle motion when energized (see Figure 2.a), and Atomic Beam Source (ABS) producing either polarised hydrogen or polarised deuterium as target (see Figure 2.b).

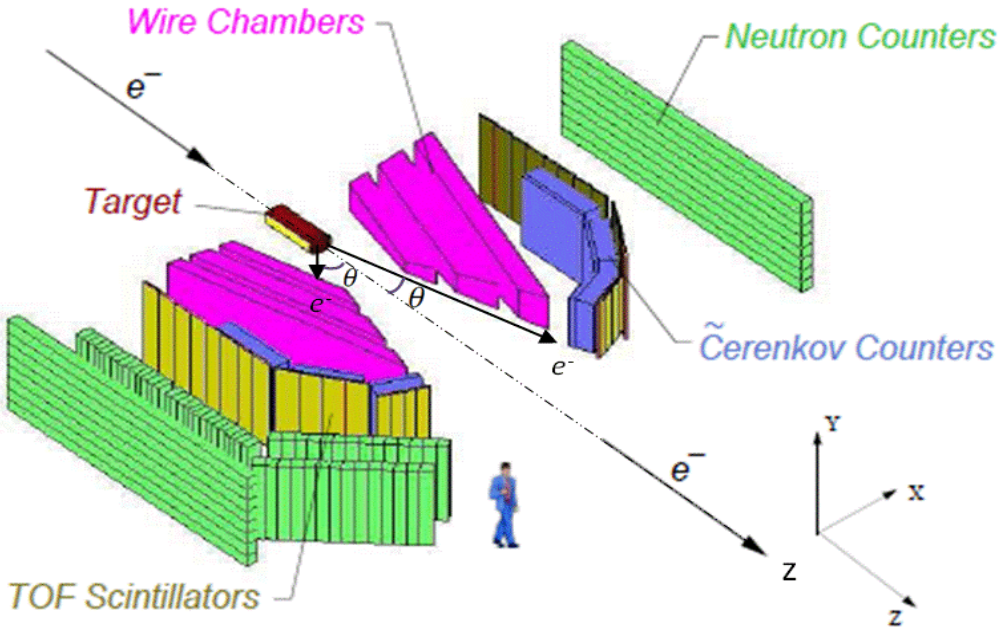


Figure 1: BLAST spectrometer and components [3].

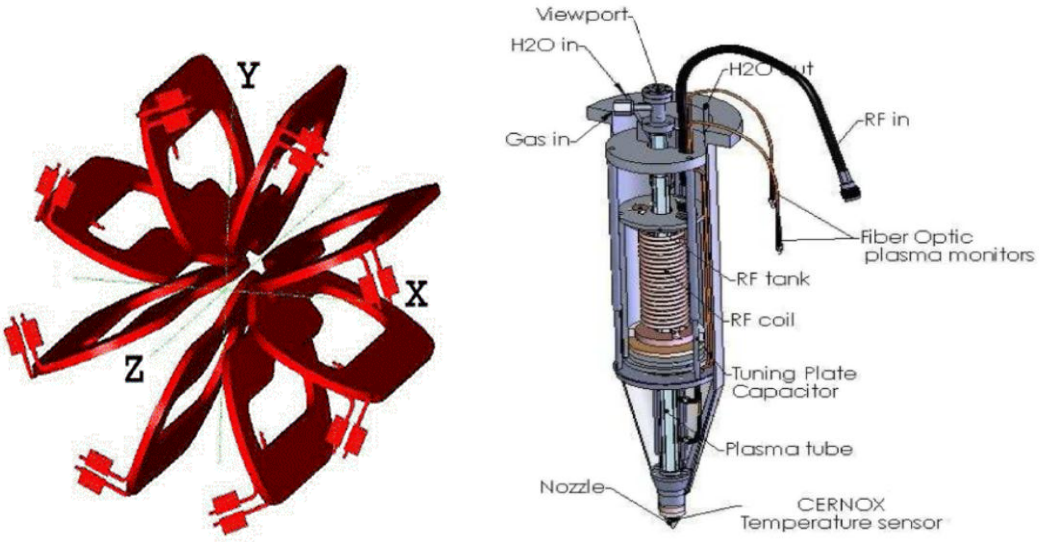


a b

Figure 2: a. Toroid magnet supplying 2 kG magnetic field along the paths of particles [4].
b. Dissociator system of the ABS [1].

### 3. Data Structure and Determination of Scattered Electrons

Various physical quantities of the particles are recorded in data files as parameters. One should know which parameter in data corresponds to which physical quantities prior to analysis. For this work, it is crucial to identify electrons scattered from target. Below, parameters which help distinguish those electrons will be explained.

#### 3.1 Particle Identification Number (PID)

For every particle type detected in the spectrometer, a particle identification (PID) number is assigned (Figure 3). The identification process is based on the track left by a detected particle in the drift chambers especially with the BLAST magnetic field turned on and timing information obtained from TOF counters. The shape of the curveture of the track lets one know the charge of the particle. The measured curveture radius lets one to obtain the momentum of the particle. In addition, the velocity of the particle is obtained using curveture length divided by the the measured time. In turn, the momentum and the velocity allows one estimate the mass of the particle. Based on the mass and the charge information the particle is identified and is tagged with the corresponding PID number. According to histogram, electron has PID 3 while positron has PID 2.

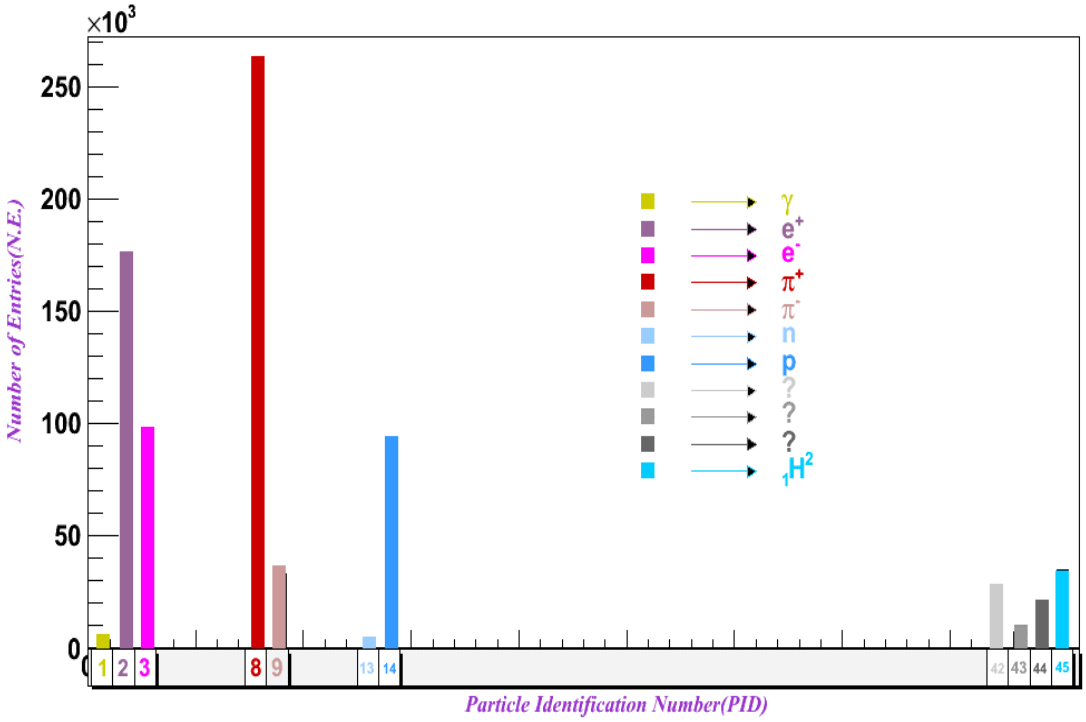


Figure 3: Distribution of detected particles based on their Particle ID numbers [5].

### 3.2 Angular Acceptance of BLAST

BLAST covers a certain range of angular acceptance which can be specified by polar ($\theta$) and azimuthal ($\phi$) angles. Selection of coordinate axes and a view from incoming electrons are shown Figure 4.

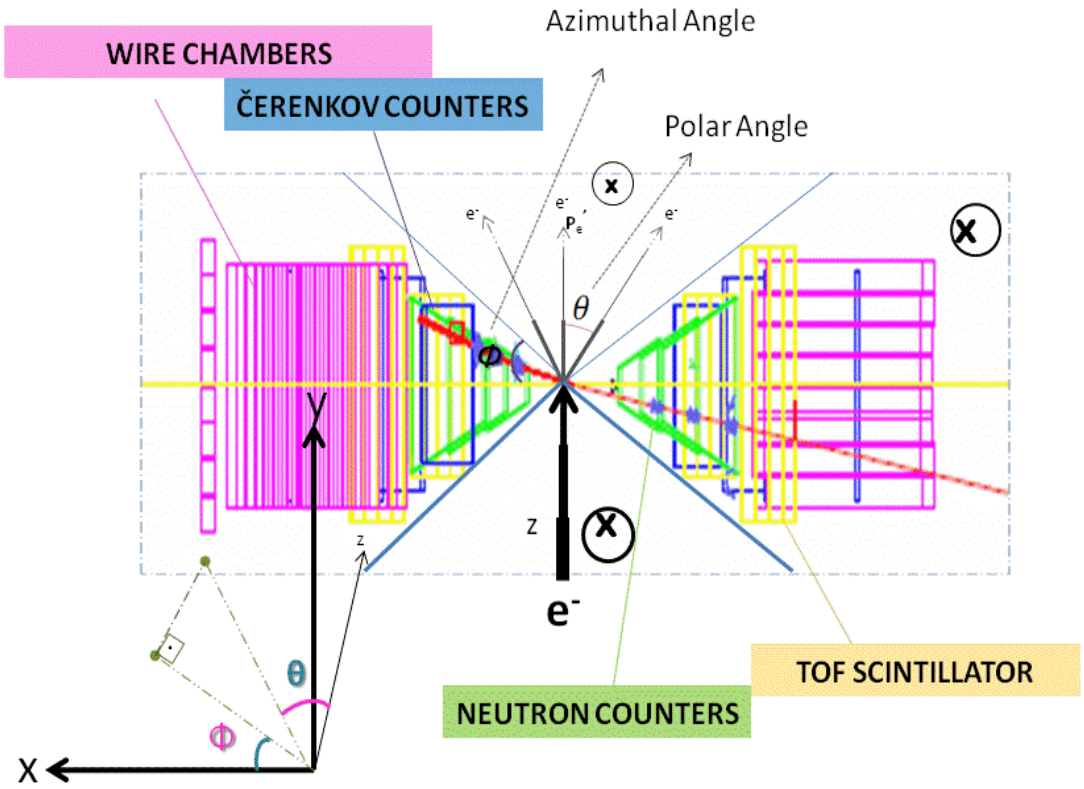


Figure 4: Kinematic quantities [5-6].

$\theta$ is the angle between incoming and outgoing electrons and $\phi$ is the angle between the x axis and the projection on x-y of direction of outgoing electrons. For BLAST, $\theta$ and $\phi$ range $20^0 - 90^0$ for both sectors, and $(-15^0) - (15^0)$ for left and $165^0 - 195^0$ for the right sector, respectively (Figure 5 – 6).

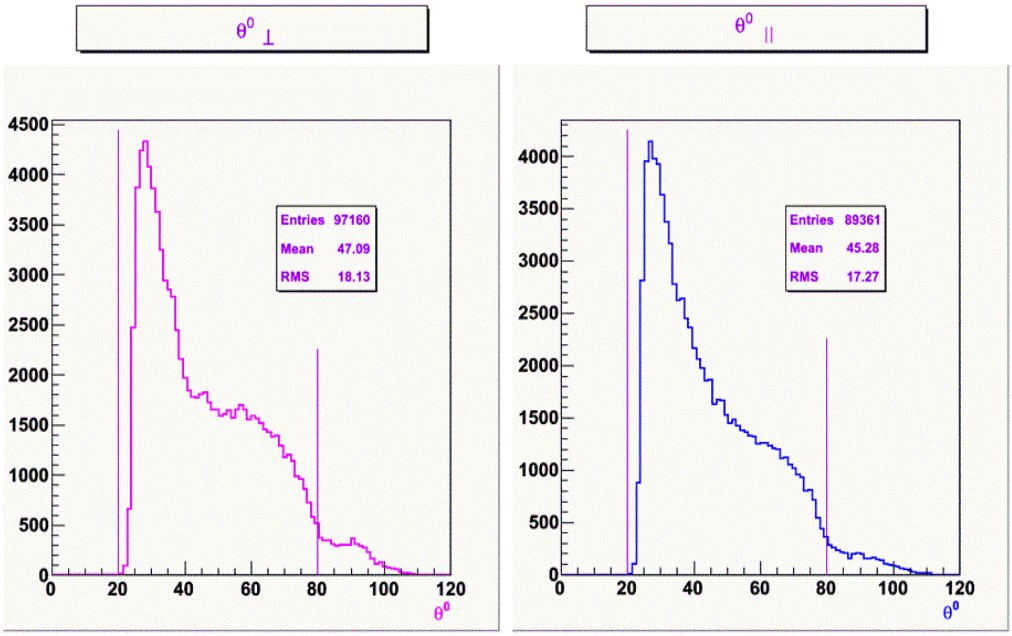


Figure 5: Polar angle ( $\theta$ ) distributions for BLAST system acceptance for perpendicular (on the left) and parallel (on the right) kinematics [5].

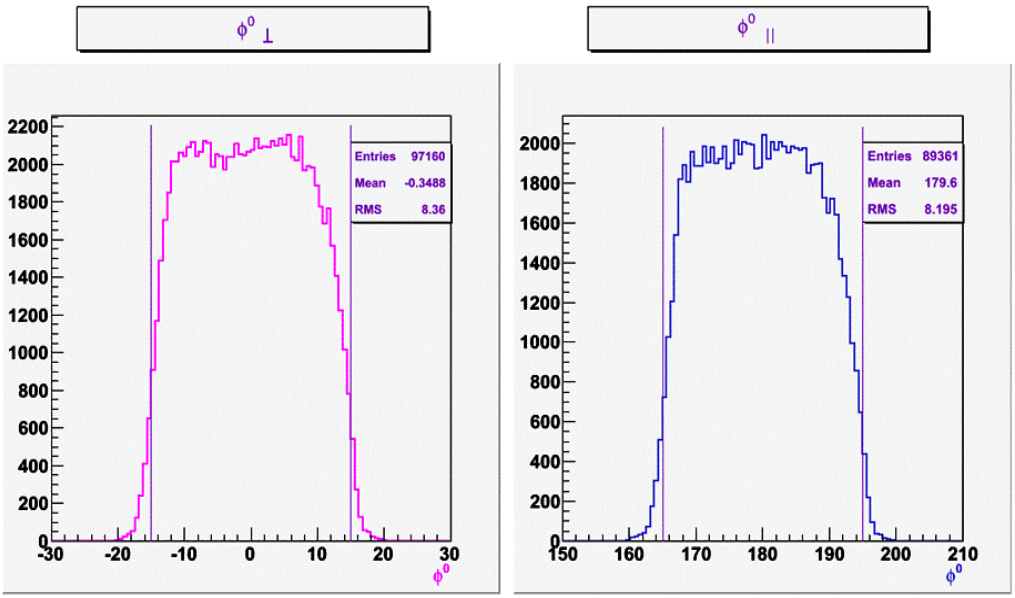


Figure 6: Azimuthal angle ( $\Phi$ ) distributions for BLAST system acceptance for perpendicular (on the left) and parallel (on the right) kinematics [5].

### 3.3 Electrons From Target

Electrons detected at BLAST system are required to satisfy the condition to come from target. Parameter "z" in data is used for this purpose. It provides the z component of the interaction vertex and is obtained by a reconstruction procedure which involves an extrapolation of the electron trace left in the detection system taking the BLAST magnetic field into account. Target is in tube shape with 60cm long and 1.5cm in diameter positioned on z axis where $z = 0$ corresponds to the center of the target. Therefore, the values of z components of the target vary from -30cm to 30cm. z distribution of the scattered electrons for both kinematics are shown in Figure 7. According to the distributions most of the electrons come from the target region.

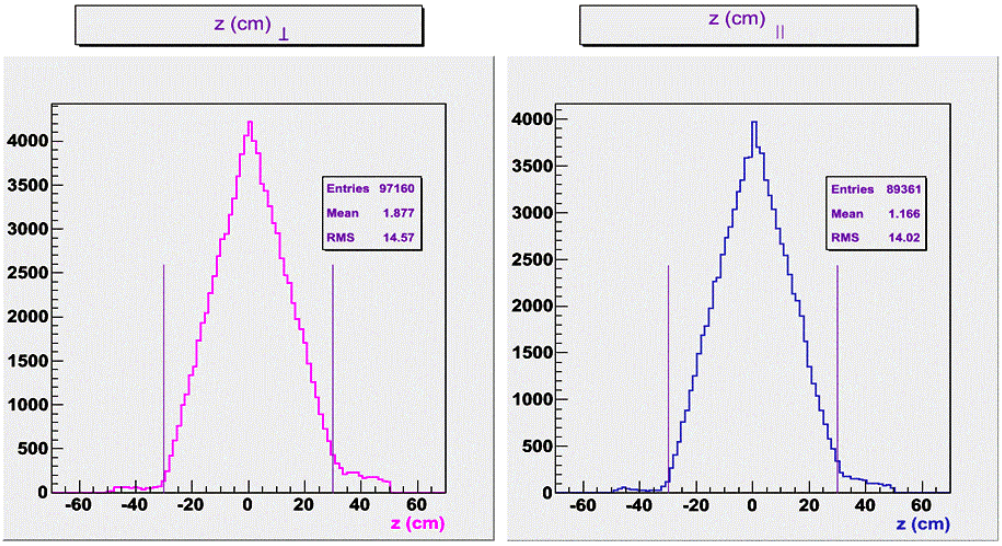


Figure 7: Showing z distributions of the scattered electrons for perpendicular (on the left) and parallel (on the right) kinematics [5].

### 3.4 Background Subtraction

Momenta of the scattered electrons are kept between $0.25\ \mathrm{GeV/c}$ and $0.85\ \mathrm{GeV/c}$ (Figure 8). Since momenta of most of the background electrons are below $0.25\ \mathrm{GeV/c}$, this value is chosen as the sub-limit of the range [4]. On the other hand, conservation of momentum dictates that the momenta of the scattered electrons be less than $0.85\ \mathrm{GeV/c}$, the value of the initial momentum of the electrons before they hit the target.

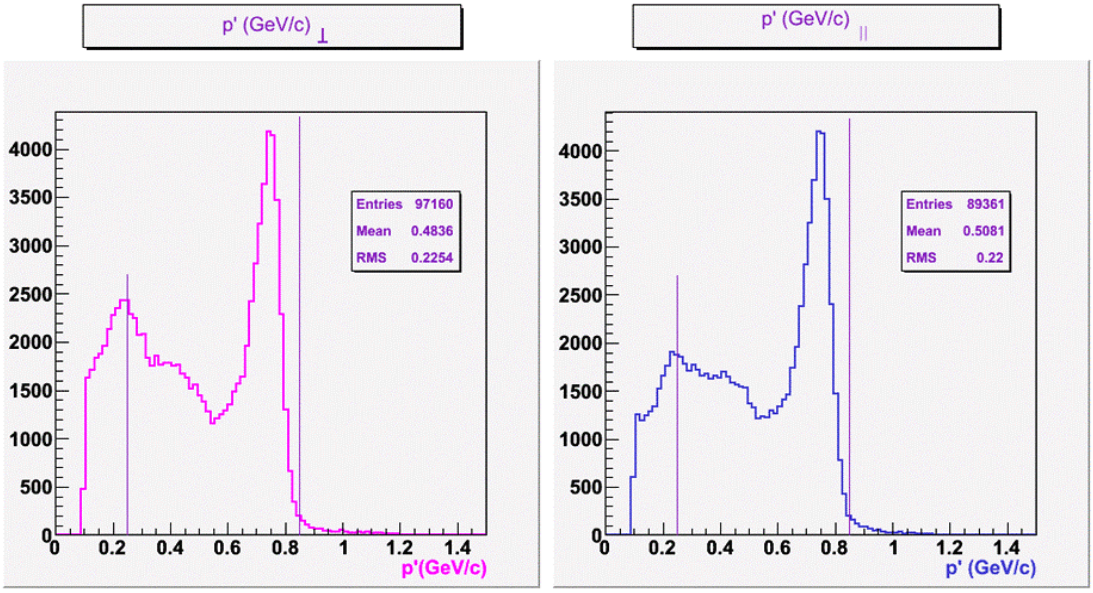


Figure 8: Momenta ( $p'$ ) distributions of the scattered electrons for perpendicular (on the left) and parallel (on the right) kinematics [5].

### 3.5 Formalism

The polarized electron-polarized deuteron scattering reaction can be written in general as

$$\vec{e}^{-} + \vec{d} -> e^{-} + X \ . \qquad (1)$$

In fact, incident beam of electrons with energy $\sim 1$ GeV can easily probes deuteron and can interact with one of its nucleon. The symbolic representation of electromagnetic channel of this reaction is shown in Figure 9.

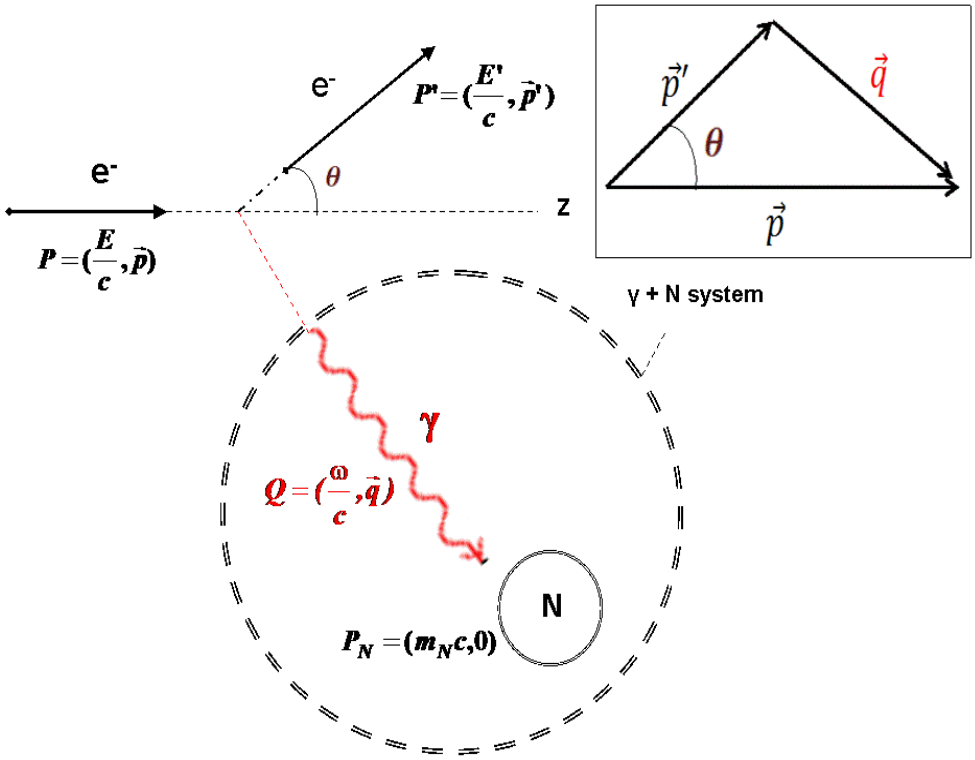


Figure 9: Symbolic representation of an electron scattered electromagnetically from one of the deutron's nucleons in the lab frame [5].

From the upper right corner of the scheme the three vector momentum transfer $\vec{q}$ carried by the virtual photon exchanged is

$$\vec{q} = \vec{p} - \vec{p}', \tag{2}$$

where $\vec{p}$ and $\vec{p}'$ are the initial and the final momenta of the electrons before and after the scattering, respectively. Based on this, three momentum transfer squared $q^2$ can be obtained by dot product of $\vec{q}$ with itself (Eq. 2) as

$$q^2 = p^2 + p'^2 - 2pp'\cos\theta, \tag{3}$$

where $\theta$ is the scattering angle of the outcoming electron.

Similar to $\vec{q}$, the four vector momentum transfer $Q$ is

$$Q = P - P', \tag{4}$$

where $P$ and $P'$ are the initial and the final four vector momenta of the electrons before and after the scattering, respectively. $P$ and $P'$ in terms of energies and three vector momenta are

$$P = (E, \vec{p}) \text{ and } P' = (E', \vec{p}'), \tag{5}$$

here c will not be shown explicitly in the expressions for it can be absorbed in the units. $Q$ can be reexpressed as

$$Q = (\omega, \vec{q}), \tag{6}$$

where $\omega$ is virtual photon energy and is given in terms of the incident electron beam energy $E$ and the scattered electron energy $E'$ by

$$\omega = E - E'. \tag{7}$$

Four momentum vector transfer squared $Q^2$ is obtained again by dot product of $Q$ with itself as

$$\left|Q^2\right| = 4EE'\sin^2(\theta/2). \tag{8}$$

In the electromagnetic interaction above, the virtual photon ( $\gamma$ ) is emitted by the electron and is subsequently absorbed by one of the nucleons of deuteron (Figure 9). As a result, the nucleon ( $N$ ) may be excited to a resonance ( $N^*$ ) , a short-lived semibound state, and the process can be represented by

$$\gamma + N -> N^*. \tag{9}$$

The scattering reaction cross-section increases substantially at the energy corresponding this resonances [7]. For investigating presence of such resonances, total four vector momentum of $\gamma + N$ system $P_T$ must be taken into account and is given by

$$P_T = P_\gamma + P_N, \tag{10}$$

where $P_\gamma$ is virtual photon four momentum and equals to $Q$ , and $P_N$ is the target nucleon's four vector momentum assumed to be at rest and hence, equals to $(m_N,0)$. The dot product of $P_T$ with itself is a Lorentz invariant and can be defined as

$$P_T.P_T = W^2, \tag{11}$$

where $W$ is called invariant mass and it is the total mass of the $\gamma + N$ system. If Eq. 10 is used in the Eq. 11, the explicit form,

$$W = \sqrt{2pp'(\cos\theta - 1) + 2(p - p')m_N + m_N^2}\ , \qquad (12)$$

is obtained in terms of $p$, $p'$, $\theta$ and $m_N$. $E \sim pc$ and $E' \sim p'c$ are used to express the $W$ relation in terms of momenta. Since electrons are in the relativistic regime, such approximations should be valid.

## 4. Analysis and Results

In this study, the kinematics of scattering electrons off deuteron are worked by obtaining distributions of $q^2$, $Q^2$ and $W$ based on inclusive analysis which uses only the scattered electron. Below these will be handled individually.

### 4.1 $q^2$ Distributions

$q^2$ distributions for both sectors are shown in (Figure 10). Since $q^2$ is a function of two independent variables, namely $p'$ and $\theta$, it is not easy to foresee the behaviour of the distribution. On the other hand, one can fix either of them at a nominal value and leave the other to change freely. In this way, the behaviour of $q^2$ dependence to the latter can be predicted and compared with the data. The dependence of $q^2$ on $p'$ at $<\theta>= 40^0$ and the dependence of $q^2$ on $\theta$ at $< p'>= 0.45$ GeV / c are shown in Figure 11.

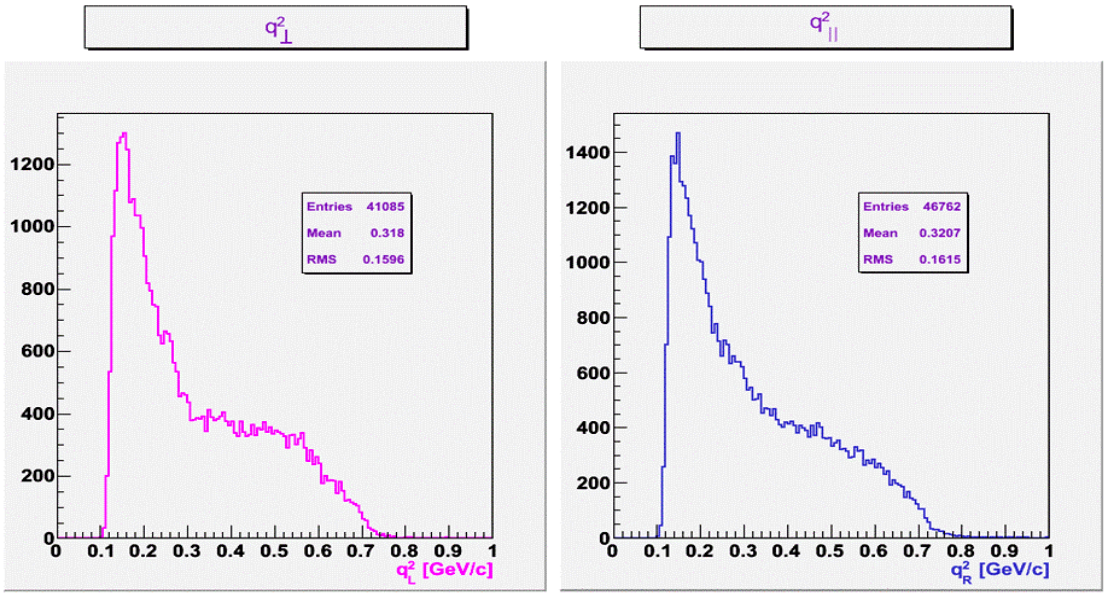


Figure 10: Three vector momentum transfer ( $q^2$ ) distributions of the scattered electrons for perpendicular (on the left) and parallel (on the right) kinematics [5].

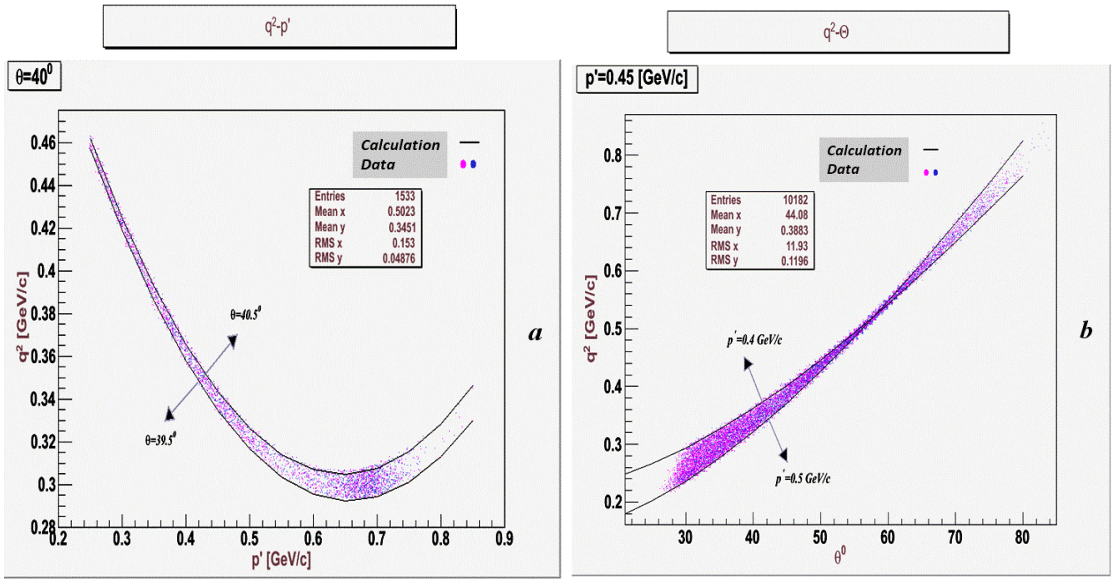


Figure 11: a. $p'$ dependence of $q^2$ at $\theta_1 = 39.5^0$ and at $\theta_2 = 40.5^0$ (calculation), and $p'$ dependence of $q^2$ distribution between $\theta_1$ and $\theta_2$ (data).
b. $\theta$ dependence of $q^2$ distribution at $p_1' = 0.4$ GeV / c and at $p_2' = 0.5$ GeV / c (calculation), and $\theta$ dependence of $q^2$ distribution between $p_1'$ and $p_2'$ (data) [5].

Each pad in the figure include two graphs and a scatter plot. The graphs show analytical results for two different values of fixed parameter and the scatter plot shows the data spread within these two values. A parabolic behaviour is expected for $q^2(p')$ based on the Eq. 5 and is observed by drawing $q^2$ for $\theta$ values of $40^0 \pm 0.5^0$ on the left pad. On the other hand, a trigonometrical behaviour is expected for $q^2(\theta)$ based on the equation and is observed by drawing $q^2$ for $p'$ values of $0.40 \pm 0.05$ GeV / c on the right pad. We can say that $q^2$ distribution is confirmed indirectly by confirming the dependencies for $p'$ and $\theta$ individually.

### 4.1 $Q^2$ Distributions

$Q^2$ distributions based on Eq. 8 for kinematics are shown in Fig. 12.

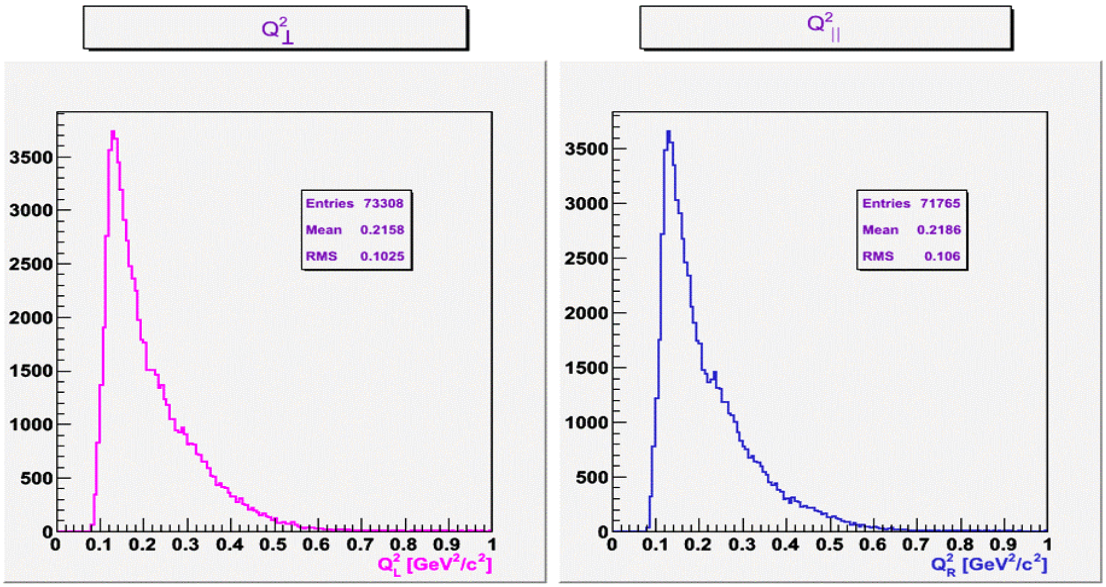


Figure 12: $Q^2$ distributions for perpendicular (on the left) and parallel (on the right) kinematics [5].

These distributions, being almost same for both kinematics, show that $Q^2$ range of BLAST is $0.1-0.6$ $(\mathrm{GeV}/\mathrm{c})^2$. Just as $q^2$, $Q^2$ also depends on both $p'$ and $Q^2$ independently. If $Q^2$ is plotted against $p'$ twice where $\theta$ is $40^0-0.5^0$ in one case and $40^0+0.5^0$ in the other, and the scatter plot based on data for both kinematics is superimposed for the range constrained by these values, a linear dependence consistent with the $Q^2$ relation (Eq. 8), is observed (Figure 13.a ). On the other hand, if $Q^2$ is treated the same way but this time for $\theta$ where $p'$ is $0.4\ \mathrm{GeV}/\mathrm{c}$, $0.5\ \mathrm{GeV}/\mathrm{c}$ and range in between, a trigonometrical behaviour, again consistent with Eq. 8, is observed Figure 13.b.

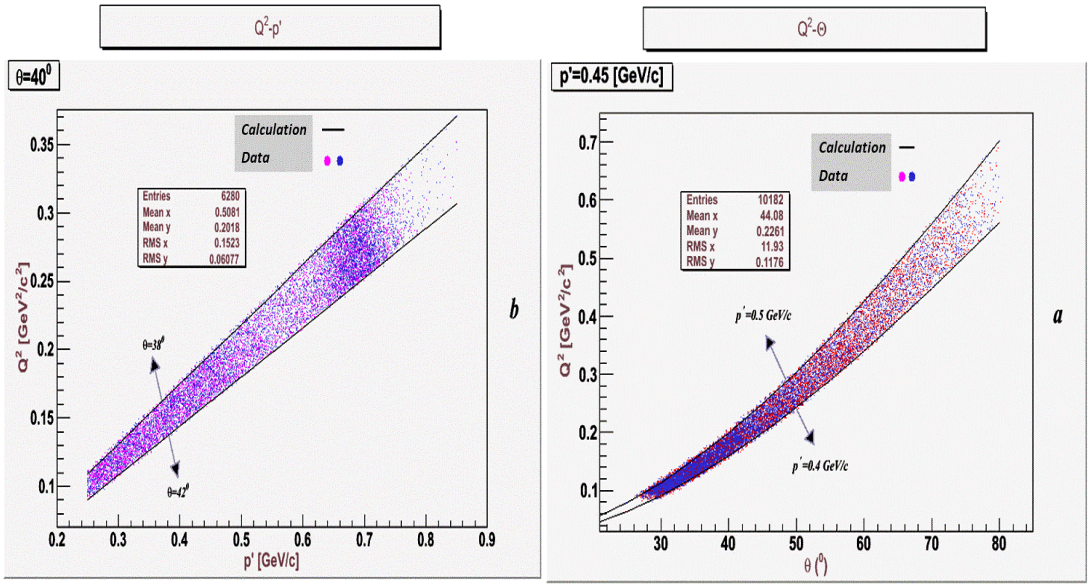


Figure 13: a. $p'$ dependence of $Q^2$ at $\theta_1 = 38^0$ and at $\theta_2 = 42^0$ (calculation), and $p'$ dependence of $Q^2$ distribution between $\theta_1$ and $\theta_2$ (data).

b. $\theta$ dependence of $Q^2$ distribution at $p_1' = 0.4$ GeV / c and at $p_2' = 0.5$ GeV / c (calculation), and $\theta$ dependence of $Q^2$ distribution between $p_1'$ and $p_2'$ (data) [5].

### 4.2 W Distributions

Invariant mass distributions for both kinematics are shown Figure 14. $W$ distributions show that $W$ range changes from 0.8 GeV / $c^2$ to 1.4 GeV / $c^2$.

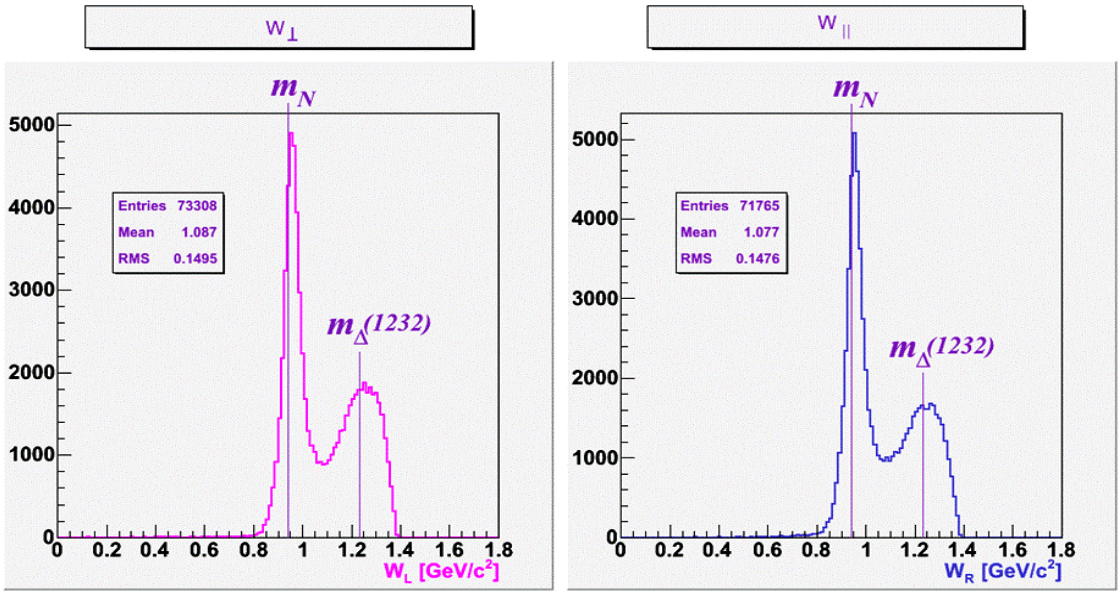


Figure 14: *W* distributions for perpendicular and parallel kinematics [5].

From the distributions, it is seen that $W$ gives two peaks: one is at $\sim 0.94\ \mathrm{GeV/c^2}$ and the other is at $\sim 1.24\ \mathrm{GeV/c^2}$. First peak being sharp and long at $W \sim m_N$ is called nucleon peak emerged from elastic events, while the second one being wide and short at $W \sim m_\Delta$, is called $\Delta$ resonance peak emerged from inelastic events. $W$ dependence to $\theta$ while $p'$ is fixed at two points, $0.435\ \mathrm{GeV/c}$ and $0.465\ \mathrm{GeV/c}$, and to $p'$ while $\theta$ is fixed at two points, $34.5^0$ and $46.5^0$, is shown seperately in Figure 15.

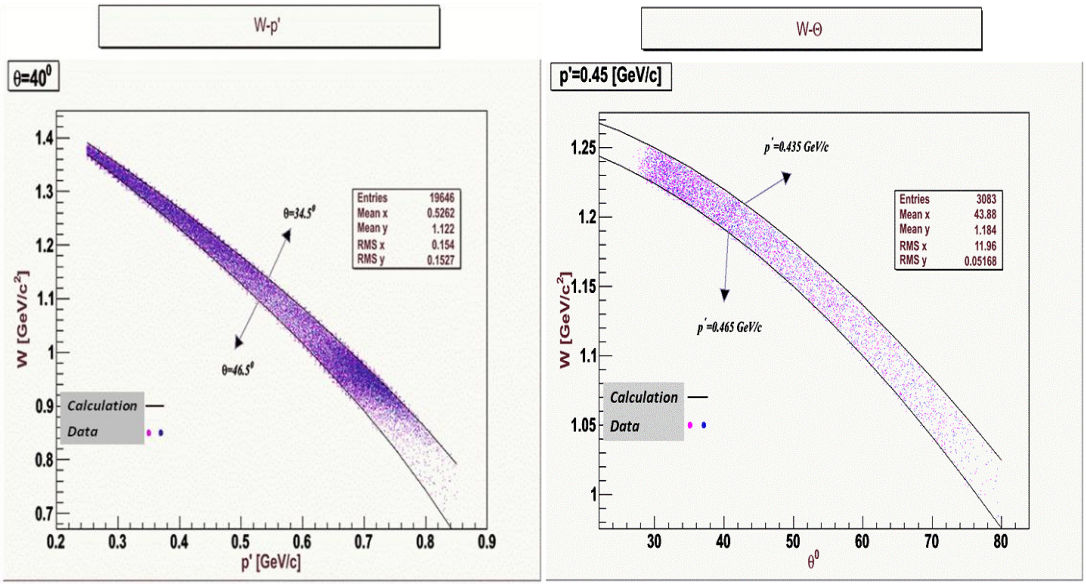


Figure 15: a. $p'$ dependence of $q^2$ at $\theta_1 = 34.5^0$ and at $\theta_2 = 46.5^0$ (calculation), and $p'$ dependence of $q^2$ distribution between $\theta_1$ and $\theta_2$ (data).
b. $\theta$ dependence of $q^2$ distribution at $p_1' = 0.435$ GeV / c and at $p_2' = 0.465$ GeV / c $GeV/c$ (calculation), and $\theta$ dependence of $q^2$ distribution between $p_1'$ and $p_2'$ (data) [5].

In both cases, line plots obtained by using fixed values in Eq. 12 and the scatter plots obtained by selecting events fall between the fixed values are compatible and show same behaviour. $Q^2$ dependence of $W$ distributions were evaluated for sub-ranges of $Q^2$ (Figure 16).

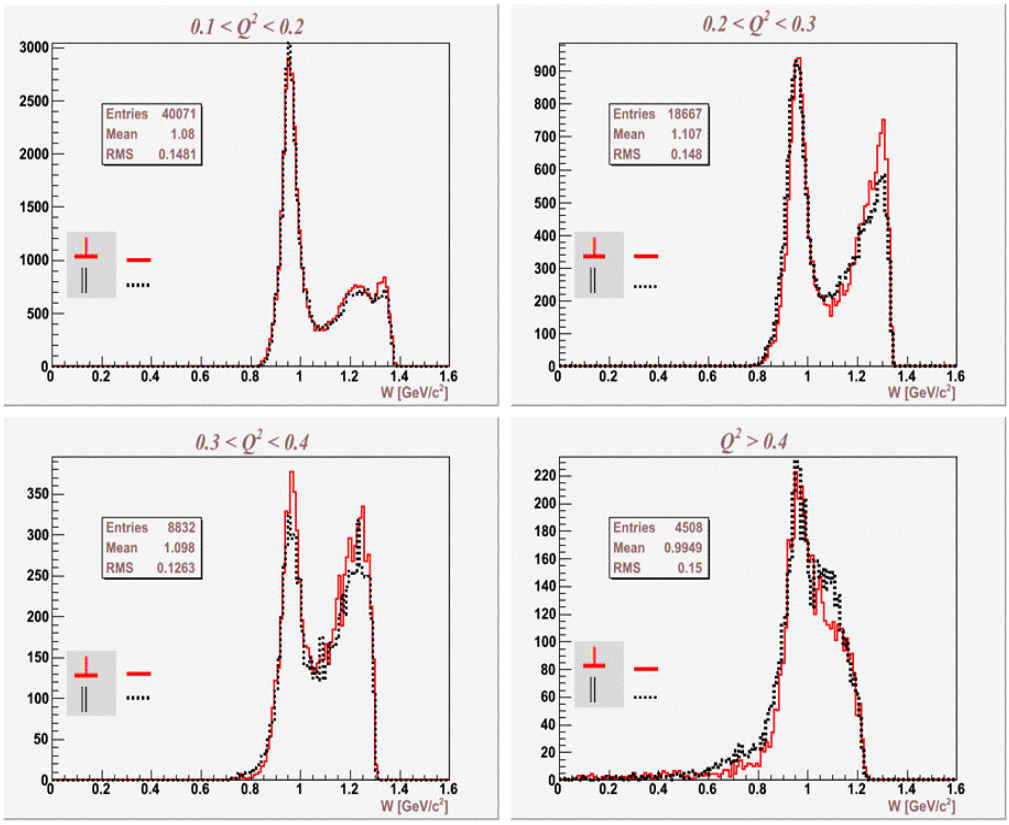


Figure 16: *W* distributions for sub-ranges of $Q^2$: $0.1 < Q^2 < 0.2$, $0.2 < Q^2 < 0.3$, $0.3 < Q^2 < 0.4$ and $Q^2 > 0.4$ $(\mathrm{GeV/c})^2$ for both kinematics [5].

By comparing elastic and inelastic peak heights, it is seen that scattering type shifts from elastic to inelastic while going from low to high $Q^2$. This result is parallel to the expectations.

**Summary and Conclusions**

Experiment of $d(e,e')X$ consists of elastic and inelastic scattering. Both scattering events are determined in this work. In all reactions, the electron beam with 850 MeV energy interacts with target nucleon assumed to be at rest by exchanging a virtual photon. 4-vector momentum transferred $Q^2$ distribution was found to be in the range of $0.1-0.6\ (\mathrm{GeV/c})^2$. *W* distributions are obtained for several sub ranges of $Q^2$. The long and sharp peak shows the elastic part of the scattering near the nucleon mass ($\sim 0.938\ \mathrm{MeV/c^2}$) in the range of $0.8-1.1\ \mathrm{GeV/c^2}$ while the wide and short peak shows the inelastic part of the scattering near the delta mass ($\sim 1.232\ \mathrm{MeV/c^2}$) in the range of $1.1-1.4\ \mathrm{GeV/c^2}$. Due to the shortness of the delta particle's lifetime ($\sim 10^{-23}\ s$), it decays before it is identified by detectors. Finally, this study will allow us to extract the delta region and will enable us to tune in either $\Delta^0$ or $\Delta^+$ resonances or both.

**Acknowledgements**

This work has been supported by the United States Department of Energy under Cooperative Agreement DE-FC02-94ER40818, National Science Foundation Grant No. PHY-0855584 and is supported by Sakarya University, Research Fund, Project No: 2011-50-02-017.

**REFERENCES**

[1] N. Meitanis, A Measurement of The Neutron Mgnetic Form Factor $G_M^n$ From Quasi-elastic $^2\vec{H}(\vec{e},e')$ at low $Q^2$, Ph.D. Thesis, Massachusetts Institute of Technology 2006.

[2] D. Hasell et al.,Nucl. Instr. And Meth. A 603, 247 2009.

[3] C. B. Crawford, Precision Measurement of the Proton Electric to Magnetic Form Factor Ratio with BLAST, Ph.D. Thesis, Massachusetts Institute of Technology 2005.

[4] O. F. Filoti, Inclusive Scattering of Polarized Electrons from Polarized Protons in the Excitation Region with BLAST, Ph.D. Thesis, University of New Hampshire 2007.

[5] S. Citci, Research Proposal, Sakarya University 2010.

[6] P. J. Karpius, Vector Polarization Observables of the Deuteron and a New Measurement of the Magnetic Dipole Form Factor $G_M$, Ph.D. Thesis, University of New Hampshire 2005.

[7] D. J. Griffiths, Introduction to Elemantary Particles, John Wiley-VCH Verlag GmbH&Co.KGaA 2008.

[8] N. Ir et al, The Extraction of the Invariant Mass Spectrum from the Electron-Deuteron Scattering by Inclusive Analysis of the BLAST Data, Science Journal, Sakarya University, 15, 1, pp. 23-29 2011.

[14] M. S. Fallon and A. Chauhan, Journal of Colloid and Interface Science, 300, 7-19, 2006.

[15] J. Kornhuber, A. W. Henkel, T. W. Groemer, S. Städtler, O. Welzel, P. Tripal, A. Rotter, S. Bleich and S. Trapp, J. Cell. Physiol., 224, 152-164, 2010.

[16] S. M. Sharker, A. A. Rahman and M. A. Alam, Insight Pharmaceutical Sciences, 1 (2), 24-28, 2011.

[17] G. Zimmer and P. Schulze, Drug Res., 31 (II), 1389-1392, 1981.

[18] P.W. Wertz and B. Bergh, Chem. Phys. Lipids, 91, 85-96, 1998.

[19] D. Marsh and K. Schorn, Biological Magnetic Resonance: 14, Spin Labeling The Next Millenium, Editor L. J. Berliner, Plenum Press, New York, 405-409, 1998.

[20] J. Strancar, T. Koklic and Z. Arsov, J. Membr. Biol., 196, 135-146, 2003.

[21] J. Strancar, T. Koklic, Z. Arsov, B. Filipic, D. Stopar and M. A. Hemminga, Journal of Chemical Information and Modeling, 45, 394-406, 2005.

[22] J. Mizushima, Y. Kawasaki, T. Tabohashi, T. Kitano, K. Sakamoto, M. Kawashima, R. Cooke and H. I. Maibach, Int. J. Pharm., 197, 193-202, 2000.

[23] T. Ogiso, T. Hirota, M. Iwaki, T. Hino and T. Tanino, Int., J. Pharm., 176, 63-72, 1998.

[24] D. J. Moore, M. E. Rerek and R. Mendelsohn, Biochem. Biophys. Res. Commun., 231, 797-801, 1997.

[25] J. Caussin, G. S. Gooris, M. Janssens and J. A. Bouwstra, Biochim. Biophys. Acta, 1778, 1472-1482, 2008.

[26] C. J. Högberg, A. Maliniak and A. P. Lyubartsev, Biophys. Chem., 125, 416-424, 2007.

[27] D. Bemporad, C. Luttmann and J. W. Essex, Biochim. Biophys. Acta, 1718, 1-21, 2005.